

Impact of Alkali Pretreatment on the Chemical Component Distribution and Ultrastructure of Poplar Cell Walls

Zhe Ji,^a Zhe Ling,^a Xun Zhang,^a Gui-Hua Yang,^b and Feng Xu^{a,*}

Alkali pretreatment is one of the leading pretreatment technologies for biofuel applications. The histochemical and structural characteristics of poplar cell walls were investigated before and after sodium hydroxide pretreatment (121 °C, 2%) to understand the alterations in biomass cellular structure, which were correlated with saccharification yield. Results showed that alkali pretreatment preferentially removed lignin from the S2 of fibers, which was similar to the behaviors of coniferyl alcohol and aldehyde (lignin-CAA), exhibiting a positive correlation between removal of the two structures. Additionally, the cellulose microfibril angle was enlarged as the residence time increased during pretreatment. Scanning electron microscopy (SEM) analysis further suggested that pretreatment caused ultrastructure changes in cell walls with cracks formation on cell wall surface, especially in the areas adjacent to the cell corner middle lamellar (CCML). Accordingly, the cellulose digestibility of residues increased from 32.1% for the raw material to 53.7% for the treated samples obtained in 72 h. It can be concluded that the changes in topochemistry and ultrastructure of poplar cell walls resulting from alkali pretreatment mediated the efficiency of enzymatic hydrolysis of residues.

Keywords: Poplar cell walls; Lignin; Coniferyl alcohol and aldehyde; Cellulose orientation; Confocal Raman microscopy

Contact information: a: Beijing Key Laboratory of Lignocellulosic Chemistry, Beijing Forestry University, Beijing, 100083, China; b: Key Laboratory of Paper Science and Technology of Ministry of Education, Qilu University of Technology, Ji'nan, 250353, China; *Corresponding author: xfx315@bjfu.edu.cn

INTRODUCTION

Plant cell walls are the most abundant renewable resource of fibrous material. Utilization of this lignocellulosic biomass as an alternative for fossil fuel, chemicals, and materials has gained much interest in the current world with diminishing amounts of fossil oil and the greenhouse effect on the environment (Holopainen-Mantila *et al.* 2013). Typically, plant cell walls are chemically inhomogeneous in major components of cellulose, hemicelluloses, and lignin within rigid cell walls. Cellulose made up of (1-4)- β -glucopyranose units is a highly crystalline polymer that is arranged in microfibrils providing a reinforced supportive layer in plants (Ciesielski *et al.* 2014). The hydrophobic and chemically durable lignin polymer is associated with hemicelluloses heterogeneously distributed within distinct morphological cell wall regions coating the surface of microfibrils (Somerville *et al.* 2004). These complicated features render biomass recalcitrant to hydrolysis into individual glucose subunits which can be further utilized for biofuel production. Therefore, the natural lignocellulosic biomass needs to be modified to make cell wall structure opened in a cost-effective process in industrial

application (Pauly and Keegstra 2008). To achieve this, various pretreatment technologies have been explored for better sugar release performance during enzymatic hydrolysis, such as thermal, biochemical, mechanical, and biological treatments (Murnen *et al.* 2007). Pretreatment is the key to disrupt or remove the cross-linked matrix of lignin and hemicelluloses that embeds the microfibrils, as well as to increase the porosity and surface area of substrates for enhancing enzymatic digestibility (Mosier *et al.* 2005).

Considering the presence of lignin is one of the primary barriers to efficient enzymatic breakdown of biomass to sugars, the alkaline delignification pretreatment has drawn much attention in past decades (McIntosh and Vancov 2011; Nlewem and Thrash Jr. 2010; Sendich *et al.* 2008). A wealth of information on the selection of operating conditions and design of pretreatment equipments has been explored in the literature (Persson *et al.* 2009; Saha and Cotta 2006; Varga *et al.* 2002), yet there is no consensus about the mechanism of alkali pretreatment at the cellular level. In addition, its performance on cell walls may vary with feedstock types. The knowledge of how poplar tissues respond to alkali pretreatment and affect the subsequent enzymatic hydrolysis is still lacking. The insufficient information on this issue provides motivation to improve the understanding of specific chemical and physical attributes of plant cell walls under pretreatment. Mooney *et al.* (1998) suggested that in addition to the amount of components, their location was another important factor affecting hydrolysis. For instance, the globular structure rich in hemicelluloses and lignin on a cell wall surface may have detrimental impacts in the enzymatic hydrolysis by limiting enzyme access to cellulose as physical barrier and tending to irreversibly bind to enzymes (Chu *et al.* 2010). Furthermore, a current study proposed a new viewpoint that apart from lignin, the precursors of lignin defined as coniferyl alcohol and aldehyde (joint abbreviation lignin-CAA for both structures) have been shown to inhibit the process of pretreatment and enzymatic degradation of cell walls (Grabber 2005; Hänninen *et al.* 2011). In earlier studies, a better understanding of the synthesis of biomass lignin and lignin-CAA was developed, while a few studies focused on the fate of lignin and lignin functional groups during pretreatment due to their relatively effortless distinction in the wood and deficiency in the tools. We report here a new approach employing confocal Raman microscopy to spatially map the ring-conjugated ethylene units distribution (Agarwal 1999; Agarwal and Ralph 2008), as well as lignin and cellulose in plant cell walls without any need for destructive handling and fixative procedures. With advantages of label-free and simple operation, it has a high sensitivity for providing position-resolved images based on a characteristic Raman band.

In the present study, a broader look at how poplar cell wall structure is modified in response to alkali pretreatment was carried out by Raman imaging and scanning electron microscopy. Specifically, we determined the dynamic distribution of lignin and lignin-CAA, the cellulose microfibril orientation, as well as the sugar release performance to dig out the relation between microscopic structure and enzymatic digestibility of alkali pretreated poplar. To our knowledge, it is the first attempt to unfold the cellulose molecular changes following pretreatments by Raman imaging. The direct visualization of these real-time modifications at a cellular level is bound to yield fresh knowledge on the mechanism of alkali pretreatment and its efficiency for resultant enzymatic hydrolysis, whereby an integrated and efficient industrial process can be tailored for specific purposes.

EXPERIMENTAL

Materials

A 4-year-old fresh poplar sample was collected from a local experimental forest at Beijing Forestry University, China. A cross-section disk 2 cm in thickness was cut from vertically growing poplar stems at breast height. The sapwood of poplar was manually cut into 1 cm × 1 cm × 2 cm blocks, and 6- μ m-thick cross sections from the native woody tissues were prepared by a sliding microtome. Chemicals used in this experiment were all purchased from Sigma-Aldrich.

Alkali Pretreatment

Sections were placed in 20 mL Teflon-lined stainless steel autoclaves together with 15 mL of 2% (w/v) sodium hydroxide aqueous solution. The closed reactors were heated in an oven for 20 min to reach the reaction temperature of 121 °C (Ucar 1990). Pretreatment was performed in triplicate at the desired temperature with residence times of 20 min and 60 min for comparison.

Confocal Raman Microscopy Measurement

The native and pretreated sections were mounted on a glass slide with a drop of water and then covered with a coverslip (0.17 mm in thickness) for Raman detection. Two-dimensional spectral images were acquired with a LabRam Xplora exquisite full-automatic confocal Raman microscope (Horiba Jobin Yvon) equipped with a motorized scan stage. For high spatial resolution, a 100 \times oil immersion microscope objective (Olympus, NA = 1.40) and a laser in the visible wavelength range ($\lambda = 532$ nm) were used. The linearly polarized laser light was focused with a nearly diffraction-limited spot size onto the samples, and the Raman signal was detected with an air-cooled back-illuminated CCD camera behind a grating spectrometer. The wavenumber ranged from 3200 to 600 cm^{-1} with a confocal aperture of 100 μm and a slit width of 100 μm . The reported depth resolution for the 400- μm confocal hole, based on the silicon (standard) phonon band at 520.6 cm^{-1} , was 2 μm . The laser power on the samples was approximately 8 mW. The lateral resolution of our system was determined via a knife-edge measurement within our sample fluid cell to be \sim 500 nm, which is not significantly lower than the theoretical limit ($0.61 \lambda/\text{NA} \approx 232$ nm). For imaging, an integration time of 3 s was chosen, and every pixel corresponded to one scan. A spectrum (scan) was acquired every 0.5 μm by averaging 2-s cycles.

For the measurement setup, imaging processing, and spectral analysis, Labspec 5 software was used. Chemical images were generated by integrating the intensity over a defined wavenumber range in the baseline-corrected Raman spectra and evaluating the area under the fitted Gaussian peaks of selected bands. The overview chemical images enabled the separation of cell wall layers differing in chemical composition and the definition of distinct regions to calculate average spectra from regions of interest for a detailed analysis. All measurements were acquired in triplicate to compare results, and the deviation of the values was less than 5%.

Field Emission Scanning Electron Microscopy (FE-SEM)

The morphology of native and treated poplar samples was analyzed using field emission scanning electron microscopy (Hitachi S-4300). Prior to acquiring images, the samples were mounted with double-sided carbon tape on pre-cut brass sample stubs and

sputter coated with a thin layer of gold. The representative images of original and pretreated poplar reported here were acquired with a 10-kV accelerating voltage at various magnifications.

Crystallinity Measurement

X-ray powder diffraction patterns of untreated and treated samples were obtained using an XRD-6000 instrument (Shimadzu, Japan). The X-ray diffractograms were recorded from 5 to 35° diffraction angle 2θ using the reflection method at a scanning speed of 5°/min with Ni-filtered Cu K α radiation ($\lambda=1.54 \text{ \AA}$) at 40 kV and 40 mA. The crystallinity index (CrI) was calculated using the following formula (Kumar *et al.* 2009),

$$\text{CrI} = (I_{002} - I_{\text{am}}) / I_{002} \quad (1)$$

where I_{002} is the counter reading at peak intensity at a 2θ angle close to 22° and I_{am} is the counter reading at peak intensity at a 2θ angle close to 16° in cellulose. $I_{002} - I_{\text{am}}$ is the intensity of the crystalline peak and I_{002} is the total intensity after subtraction of the background signal measured without cellulose. I_{am} represents the amorphous portion.

Enzymatic Hydrolysis

The native and pretreated poplar samples were enzymatically hydrolyzed in a 0.1 M sodium acetate buffer with a pH of 4.8 at a biomass loading of 10% (w/v) in an air-shaking incubator maintained at 50 °C at 150 rpm for 48 h. Commercial cellulase was purchased from Sigma-Aldrich (Shanghai, China) and employed at the activity of 15 FPU/g substrate for all samples. The reactions were monitored by taking 100 μL supernatant at specific time intervals, followed by deactivation of the enzymes in boiling water for 10 min and centrifugation at 10,000 g for 5 min. The released monosaccharides were analyzed by high-performance anion exchange chromatography (HPAEC) (Dionex, ISC 3000, USA) equipped with an electrochemical detector and CarboPac PA 20 analytical column (4 \times 250 mm, Dionex). Results are expressed as percentage of the total cellulose in the substrate. Error bars show the standard deviation of triplicate measurement. All assays were performed in triplicate. Error bars showed the standard deviation of triplicate measurements.

RESULTS AND DISCUSSION

Raman Spectral Characterization of Poplar

A Raman spectrum is composed of characteristic bands that are caused by an inelastic scattering from chemically bonded structures. As shown in Fig. 1, the average Raman spectra recorded from various morphological regions (cell corner middle lamellar (CCML), compound middle lamellae (CML), and secondary wall (S1 and S2)) of poplar fibers were primarily assigned to the major components, namely cellulose, hemicelluloses, lignin, and pectin. The intense Raman bands in the region of 2700 to 3000 cm^{-1} are attributed to the C-H and C-H₂ stretching of all plant cell wall substances, while the dominant spectral contribution in the 1570 to 1700 cm^{-1} range mostly originates from lignin, wherein the 1595 cm^{-1} band of aromatic ring C=C stretching is one of the typical Raman signals. Additionally, another predominant lignin peak is detected at 1653 cm^{-1} due to aromatic ring conjugated C=C and C=O structures, which is indicative of

lignin-CAA. The corresponding Raman bands of cellulose were mostly localized at 380, 1096, and 1121 cm^{-1} , which were known for contribution of β -D-glucosides and asymmetric and symmetric stretching vibration of C-O-C linkages, respectively. Although only the 380 cm^{-1} band has contribution from cellulose alone, it was not chosen to construct the localized Raman images due to the low signal-to-noise ratio. Considering the sensitivity of the peak at 1096 cm^{-1} to the cellulose molecule orientation, the 1090 to 1105 cm^{-1} region was used to screen the dynamic changes of cellulose distribution (Fig. 6), whereas hemicelluloses have remained undetected due to their low content and overlapping with stronger bands of other components (Agarwal and Ralph 1997).

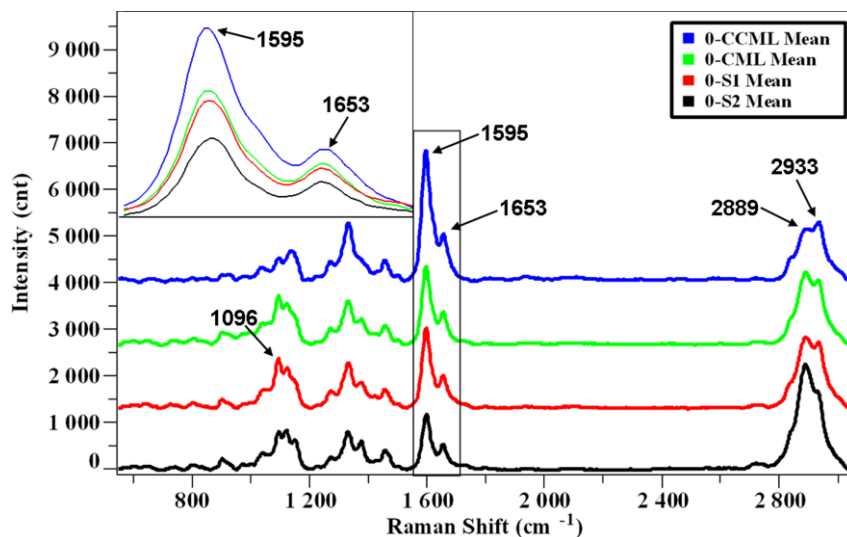


Fig. 1. Comparison of average Raman spectra acquired from the various morphologically distinct cell wall layers within poplar. Inset spectra showing a zoom into the region of 1570 to 1700 cm^{-1} .

Lignin Distribution Revealed by Raman Imaging

Lignin, interwoven with cellulose and hemicelluloses, is considered to be the primary source of natural recalcitrance in biomass conversion. By calculating the integral of corresponding marker band at 1595 cm^{-1} , the lignin distribution in various morphological regions was visualized as illustrated in Fig. 2. Within original fibers, the highest lignin signal intensity was observed in the CCML and, somewhat less in the CML, while the lowest occurred in the S2 regions (Fig. 2a). Similar results were also demonstrated by spectral analysis (Fig. 1), which was consistent with previous studies of lignin distribution in the xylem of angiosperms and gymnosperms (Agarwal 2006; Gierlinger and Schwanninger 2006; Ma *et al.* 2013).

To assess the impact of alkali pretreatment on lignin distribution, position-resolved microspectroscopic measurements were also performed by acquiring spectral images (Figs. 2b-c). As can be seen, there was strong contrast in the images of pretreated samples between morphologically distinct regions, primarily due to different rates of delignification within various wall layers. The lignin concentration in the S2 regions was significantly depleted to be almost undetectable, while there were no such substantial changes in the CCML and the CML. This phenomenon was further evidenced by the spectral comparison at the 1595 cm^{-1} band in Fig. 3, from which the magnitude of lignin removal could be quantified as 22%, 33%, and 69% in the CCML, CML, and S2, respectively. These observations indicated that there was a selective delignification in the S2 layer, due in part to the preferential penetration from the cell lumen, which has a

relatively low-density structure (Donaldson 2001; Wang *et al.* 2012) and partly because of the diverse reactivity of different lignin units in various regions (Wang *et al.* 2012).

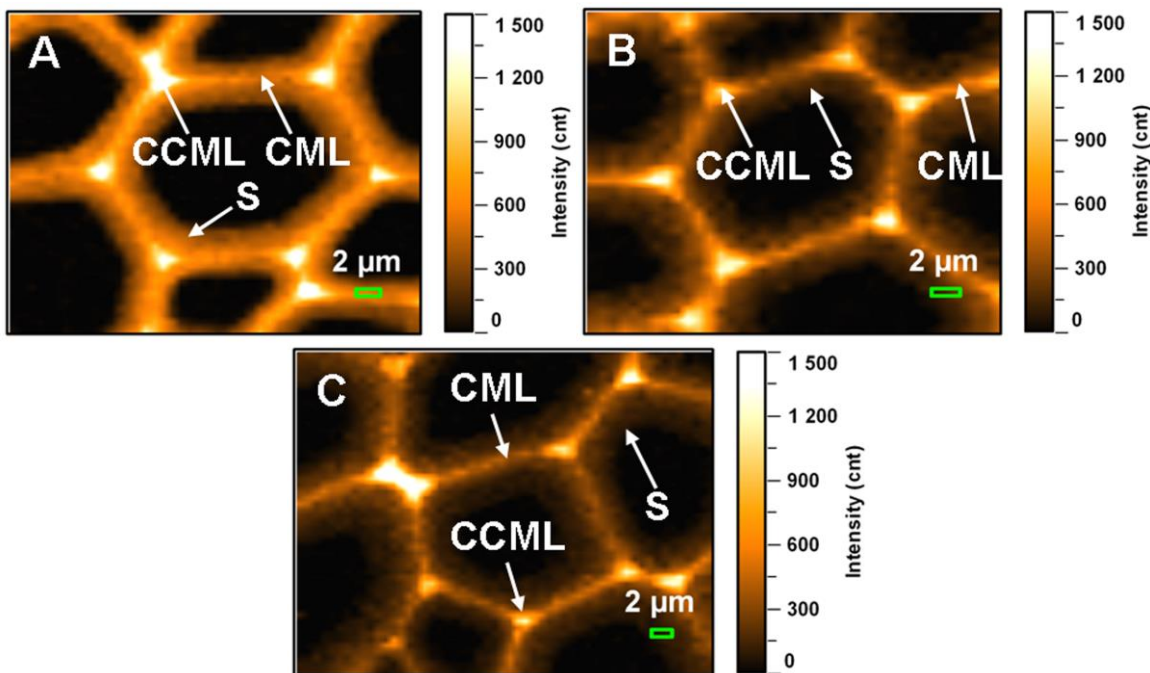


Fig. 2. Raman images showing the distribution of lignin within cell walls at different pretreatment times: 0 min (A), 20 min (B), and 60 min (C), by integrating from 1575 to 1620 cm^{-1}

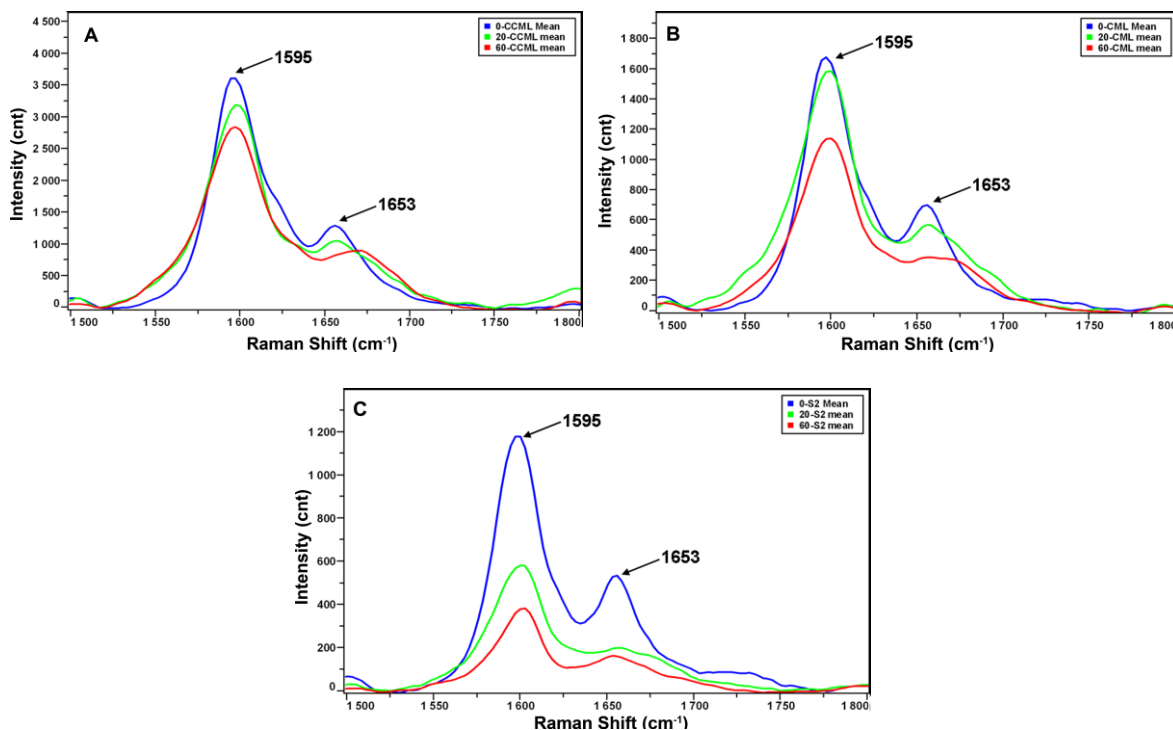


Fig. 3. Comparison of average spectra collected from various regions at different pretreatment times: CCML (A), CML (B), and S2 (C).

CAA Distribution Revealed by Raman Imaging

As an important precursor of lignin, the distributional changes of lignin-CAA during alkali pretreatment were also investigated by Raman imaging. Focusing on the region of 1640 to 1665 cm^{-1} , lignin-CAA images were generated and are shown in Fig. 4. Prior to alkali pretreatment, the heterogeneous intensity distribution was obtained within cell walls, resembling the pattern of lignin. In other words, the enrichment of lignin-CAA was localized in the lignin-enriched region CCML, whereas lignin-CAA showed an obvious deficiency in the S2, which was full of cellulose. The correlation between the distribution of lignin-CAA and of lignin in raw poplar demonstrated a linear trend at the cellular level. This finding coincided with the fact that poplar lignin in the CCML is enriched in guaiacyl units that were derived from lignin-CAA, whereas lignin in the secondary wall is typically replenished with syringyl units (Donaldson 2001; Wang *et al.* 2012). In comparison, a previous study on phloroglucinol-HCl-stained spruce by ultraviolet-visible microscopy has shown higher lignin-CAA moieties in the primary wall and S1 (Peng and Westermarck 1997). Meanwhile, another report on *Picea mariana* with respect to Raman imaging revealed no distinctions in the lignin-CAA contents within different wall layers (Agarwal 2006). Additionally, a recent study on compression wood of *Pinus bungeana* Zucc., also using Raman imaging, demonstrated that the high intensity of lignin-CAA was predominately localized in the S1 and S2 regions (Zhang *et al.* 2012). These discrepancies concerning the relationship between lignin and lignin-CAA distribution may be species-dependent. During alkali pretreatment, the changes in lignin-CAA distribution exhibited very similar features to that of lignin. Pretreatment for 20 min decreased the average Raman intensity, while the residual concentration in the CCML was still somewhat higher than that in the S2 regions and, additionally, the boundary of CML was indistinguishable (Fig. 4B). At later stages of pretreatment, the average signal intensity of total cell areas tended to disappear, while a small portion of lignin-CAA was still locked in the CCML regions (Fig. 4C).

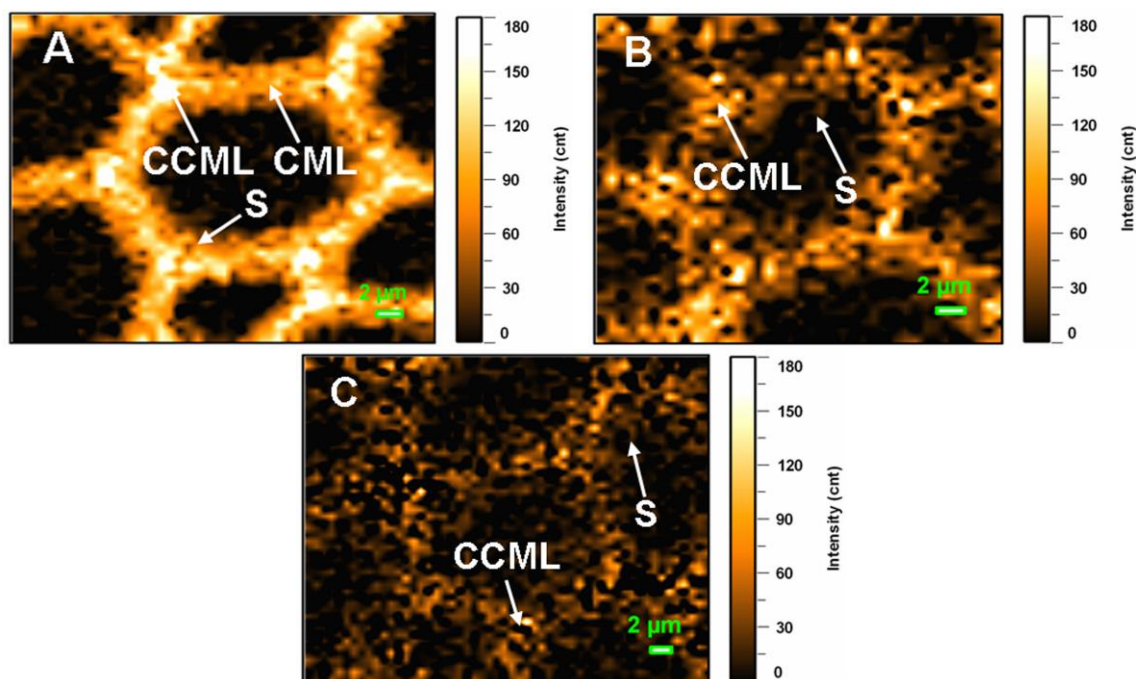


Fig. 4. Raman images showing the distribution of lignin-CAA within cell walls at different pretreatment times: 0 min (A), 20 min (B), and 60 min (C), by integrating from 1640 to 1665 cm^{-1} .

To semi-quantify the variations in lignin-CAA distribution within poplar cell walls, Raman spectral analysis was employed based on Fig. 3. As shown, along with the prominent decrease of the 1595 cm^{-1} band, great changes in the height of the 1653-cm^{-1} peak were observed in various morphologically distinct regions upon alkali pretreatment. This indicated that there was an accompanied correlation between the removal of lignin and lignin-CAA structures. Statistically, alkali pretreatment for 60 min caused intensity reductions in the range of 39% (in the CCML) to 67% (in the S2). It should be noted that there existed obvious alterations in the shape of the 1653 cm^{-1} band accompanied by a Raman shift to higher frequencies, particularly in the CCML and CML areas. One possible explanation is that new chemical structures generated in the process may have a Raman band at that wavenumber area, influencing the original peaks; *i.e.*, *p*-quinones contributing in the range of $1660\text{ to }1690\text{ cm}^{-1}$ (Agarwal *et al.* 2011). Model compound studies would be required to comprehensively address this alteration.

As previously reported, lignin is generally cross-linked with hemicelluloses that embed cellulose fibers (Abud *et al.* 2013), and lignin-CAA associates with the hydroxyl groups of cellulose and hemicelluloses *via* hydrogen bonding within cell walls (Grabber 2005). These features give rise to a mesh-like structure of plant cell walls, which contributes to the biomass recalcitrance and influences its utilization, especially for pretreatment and subsequent enzymatic degradation. Therefore, disrupting the cross-linked structures and thus increasing the accessibility of polysaccharides fractions in biomass are the prerequisites for efficient bioconversion. The holistic overview of compositional changes we have stated above will further accelerate the understanding of alkali pretreatment mechanism and the development of cost-competitive bioconversion.

Cellulose Orientation Revealed by Raman Imaging

Knowing that cellulose is a crystalline polymer and is highly oriented, restricting integration to the orientation-sensitive band at 1096 cm^{-1} could differentiate various orientations of the cellulose molecules and thereby work out the differences between samples. Before alkali pretreatment, a small layer representing the S1 was clearly separated from cell walls with higher signal intensity than the other regions because of a stronger horizontal vibration of C-O-C stretching with respect to the polarized direction in these areas (Fig. 5A). It should be noted that artifacts caused by cellulose microfibril orientation manifest themselves as darker (Y-direction) and brighter (X-direction) areas in the S1 layers. This phenomenon has been elaborated earlier by Wiley and Atalla (1987) and utilized widely in Raman imaging by Gierlinger *et al.* (2006).

During pretreatment, the Raman signal intensity in the S1 increased along with pretreatment time, while there were no obvious changes in the other morphological regions, including the CCML and S2. From a spectral perspective, if a cellulose microfibril is aligned parallel to the fiber axis in the transverse section, the observed C-O-C stretching vibration as a vertical backbone in the laser polarization direction shows low intensity, whereas the side chain methylene groups perpendicularly arranged with cellulose molecules are in plane with the incident light and present high intensity (Agarwal and Atalla 1986). In other words, when cellulose microfibrils are aligned with high microfibril angles as in the S1, the C-O-C stretching becomes more perpendicular to the fiber axis, thus enhancing the Raman signal in the laser polarization direction, as in the pretreated samples (Fig. 5C).

In terms of chemical analysis, cell walls generally consist of subunits that are connected by means of covalent and hydrogen bonds responsible for the rigid and highly compact cellulose framework within biomass (Vian 1982). Pretreatment with alkali induced cell wall swelling, consequently modified the original tendency to open or reform intra- and inter-molecular hydrogen bonding networks of polysaccharides (Shomer *et al.* 1991), leading to a rearranged supramolecular structure. Correspondingly, the orientation of C-O-C stretching may be altered to be more parallel to the laser polarization direction than before, especially in the S1. Another possible explanation could be attributed to the relatively slight increase in cellulose crystallinity from 43.9% for raw materials to 49.8% for the samples pretreated for 60 min (Table 1). This observation was further supported by the polarized images, where the S1 layer of secondary cell walls exhibited strong birefringence, indicating crystalline cellulose (Fig. S1). This increase of crystallinity in pretreated fibers may result from a removal of some of amorphous cellulose and a rearrangement of the crystalline regions (Ben Sghaier *et al.* 2012). In cell wall assembly, microfibril orientation and lignification may be mediated by changes in the amount and localization of noncellulosic polysaccharides (Donaldson and Knox 2012). Similarly, in this work, the selective removal of lignin and hemicelluloses may give rise to changes in cellulose microfibril orientation. To our knowledge, this is the first attempt to investigate the features of cellulose molecular orientation during pretreatment by the Raman imaging technique. Evaluating the effect of different degrees of these changes in poplar wood with pretreatment and the consequence of saccharification efficiency will be a future course of study.

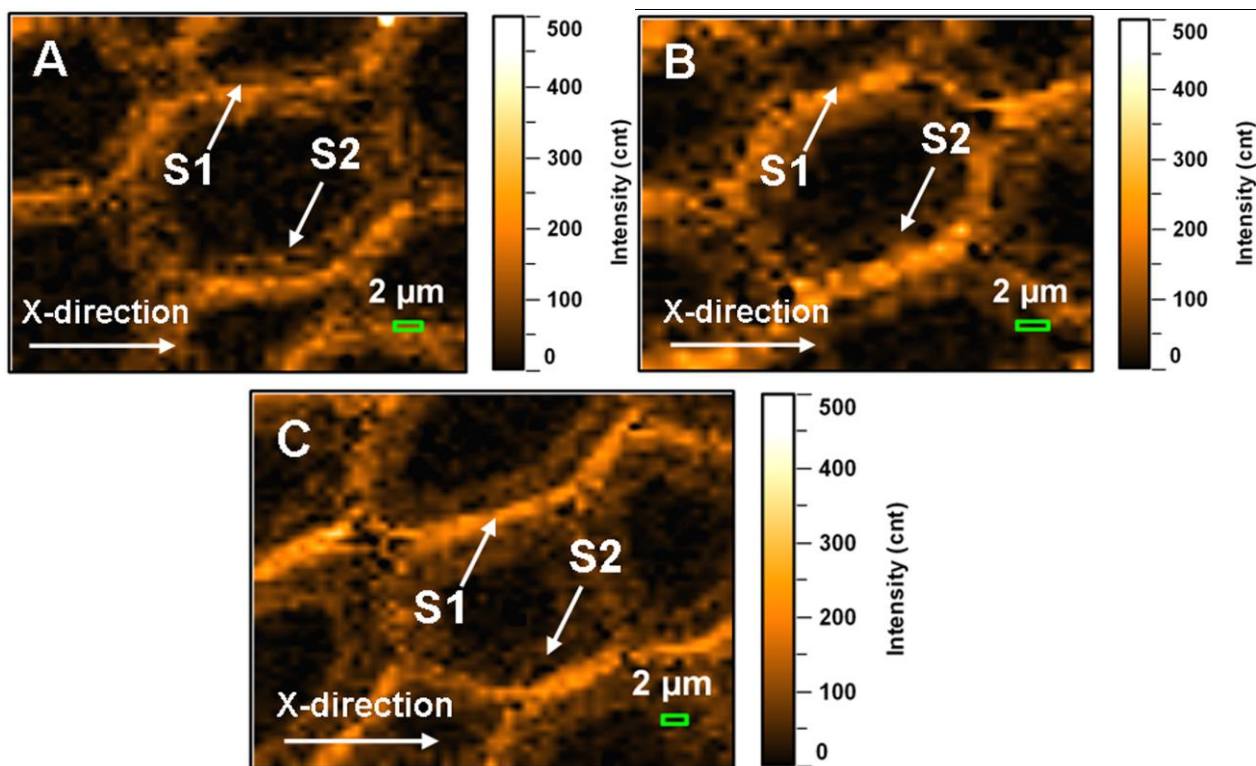


Fig. 5. Raman images showing the cellulose microfibril orientation within cell walls pretreated for different times: 0 min (A), 20 min (B), and 60 min (C), by integrating from 1090 to 1105 cm^{-1}

Table 1. Effects of Various Pretreatment Times on Biomass Crystallinity and Monosaccharide Yield

Sample	Crystallinity index (%)	Enzymatic hydrolysis	
		Glucose yield (%) ^a	Xylose yield (%) ^a
Untreated	43.9	32.1 ± 1.2	27.0 ± 1.24
121°C-20 min	48.9	45.8 ± 1.3	48.5 ± 0.98
121°C-60 min	49.8	53.7 ± 2.1	57.6 ± 1.65

^a Calculated on the basis of monosaccharide content after 72 h of hydrolysis

FE-SEM Analysis

FE-SEM images of untreated and alkali-pretreated poplar sections taken at various magnifications are shown in Fig. 6. Results showed that the raw materials had a highly intact morphology and relatively smooth cell wall surface (Fig. 6a). However, the cell wall structure was disrupted by alkali pretreatment with formation of holes and cracks on the biomass surface, especially at the boundary between CCML and secondary wall (Figs. 6b-e), whereas the original cell outline was still preserved. It is well known that lignin is essential to the structural integrity of cell walls, as well as the stiffness of plant stem and root. As a result of alkali pretreatment, lignin was largely removed from the S2; thus the natural structural traits were tailored for deconstruction. Moreover, hemicelluloses referred to as an adhesive in cell walls are enriched in the boundary of layers (Hoffmann and Parameswaran 1976). Thereby partial dissolution of hemicelluloses under alkali pretreatment further contributed to the disruption in boundary areas (McIntosh and Vancov 2011). Nevertheless, the residual lignin in the CCML and cellulose, which was considered the scaffold of cell wall structure, was still confined within cell walls to retain its original cell outline. To be clear, though slight crevices on the surface of thin cross sections induced by sampling preparation cannot be discarded, the cracks in pretreated samples were indicative of structural changes mainly due to the alkali pretreatment, which was closely related to cellulose digestibility.

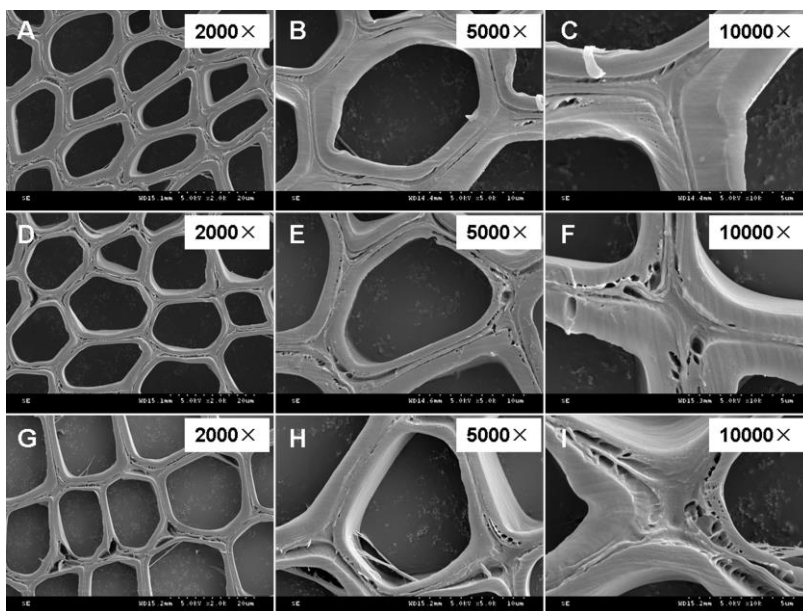


Fig. 6. SEM images showing the ultrastructural changes of poplar cell walls pretreated for different times of 0 min (A-C), 20 min (D-F), and 60 min (G-I) at various magnifications.

It has been reported that the specific surface area and the mean pore size play an important role in terms of cellulase adsorption on the cellulose surface and subsequent enzymatic deconstruction (Grethlein 1985; Yang and Wyman 2006). During alkali pretreatment, the removal of lignin and development of cracks not only could increase the cellulose fibril accessibility, but also provided more available enzyme binding sites, which therefore substantially accelerated the biodegradation process. These results suggest that effective pretreatment is essential to open the plant cell wall structure and expose cellulose fibrils, facilitating the hydrolysis yields of alkali pretreated biomass as discussed as follows.

Enzymatic Hydrolysis of Pretreated Poplar

Enzymatic hydrolysis of both untreated and alkali pretreated poplar to reducing sugar was carried out to compare their hydrolysis kinetics and cellulose digestibility. Figure 7 shows the cellulose digestibility profiles for untreated and pretreated samples at the enzyme loading of 15 FPU/g substrate. As expected, for untreated wood low hydrolysis ratio (30.3%) was observed within 48 h, whereas alkali treated poplar for 20 min achieved higher saccharification kinetics, with cellulose digestibility reaching 42.6% over the same time interval. After progressive pretreatment for 60 min, a maximum improvement of 21.6% in glucose yield was observed as compared with raw materials and up to 53.7% after 72 h of hydrolysis. Similar to the increase in glucose yield for the pretreated samples, the xylose release performance was also greatly enhanced (Table 1). Although it was not the immediate substrate target of the cellulase cocktail, xylose was considerably liberated from the pretreated biomass by the contaminating xylan-hydrolyzing enzymes present in the commercial enzyme preparation. The overall improvement in hydrolysis rates and yields from pretreated polar was speculated to be attributable to the reduced lignin and lignin-CAA content, as well as the cracks formation. The modifications degraded the biomass recalcitrance and provided an enhancement in cellulose surface area for enzyme binding sites, and thus facilitating the cellulose digestibility of pretreated samples. The results suggested a strong correlation between the efficiency of enzymatic conversion and the topochemistry and structure of plant cell walls.

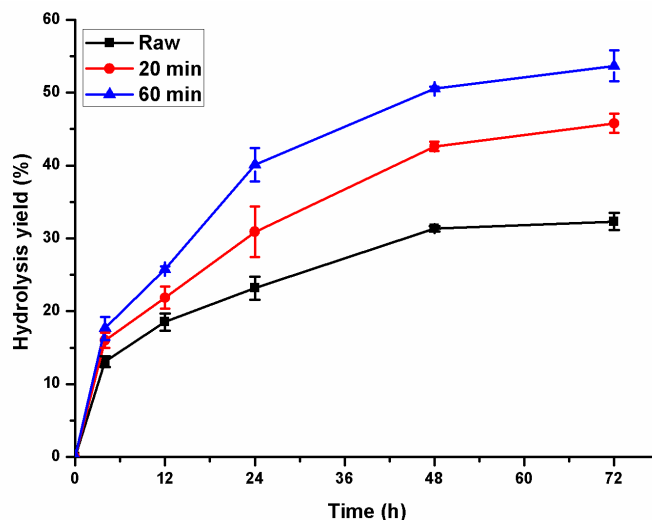


Fig. 7. Enzymatic hydrolysis of poplar pretreated with different residence times at 10% substrate concentration and enzymatic dosage of 15 FPU/g substrate

CONCLUSIONS

1. There was a positive correlation between the removal of lignin and lignin-CAA during alkali pretreatment, such that the both structures were preferentially removed from the S2 regions of fibers.
2. Pretreatment with alkali enlarged the microfibril angle, particularly in the S1 layer, as the residence time increased.
3. The formation of cracks on biomass surfaces that were adjacent to the boundary of CCML and S during alkali pretreatment could accelerate cellulose accessibility and subsequent enzymatic hydrolysis.
4. The ultrastructural and topochemical changes during alkali pretreatment greatly enhanced the rates and yields of enzymatic hydrolysis. However, considering that the samples used for microscopic measurements were 6- μm -thick cross sections, the differences between the results achieved by treating sectioned samples and sectioning samples should be taken into consideration.

ACKNOWLEDGMENTS

We gratefully acknowledge financial support from the National Science Fund for Distinguished Young Scholars (31225005) and the Chinese Ministry of Education (113014A). Additionally, the authors are grateful to the kind support from the Committee of the 4th Conference on Biorefinery towards Bioenergy (ICBB2013) in Xiamen, China.

REFERENCES CITED

- Abud, Y., Costa, L. T., Souza, W., and Sant'Anna, C. (2013). "Revealing the microfibrillar arrangement of the cell wall surface and the macromolecular effects of thermochemical pretreatment in sugarcane by atomic force microscopy," *Ind. Crops Prod.* 51(1), 62-69.
- Agarwal, U., and Atalla, R. (1986). "In-situ Raman microprobe studies of plant cell walls: Macromolecular organization and compositional variability in the secondary wall of *Picea mariana* (Mill.) BSP," *Planta* 169(3), 325-332.
- Agarwal, U. P. (1999). "An overview of Raman spectroscopy as applied to lignocellulosic materials," in: *Advances in Lignocellulosics Characterization*, D. S. Argyropoulos (ed.), TAPPI Press, Atlanta, Georgia.
- Agarwal, U. P. (2006). "Raman imaging to investigate ultrastructure and composition of plant cell walls: Distribution of lignin and cellulose in black spruce wood (*Picea mariana*)," *Planta* 224(5), 1141-1153.
- Agarwal, U. P., McSweeney, J. D., and Ralph, S. A. (2011). "FT-Raman investigation of milled-wood lignins: Softwood, hardwood, and chemically modified black spruce lignins," *J. Wood Chem. Technol.* 31(4), 324-344.
- Agarwal, U. P., and Ralph, S. A. (2008). "Determination of ethylenic residues in wood and TMP of spruce by FT-Raman spectroscopy," *Holzforschung* 62(6), 667-675.

- Agarwal, U. P., and Ralph, S. A. (1997). "FT-Raman spectroscopy of wood: Identifying contributions of lignin and carbohydrate polymers in the spectrum of black spruce (*Picea mariana*)," *Appl. Spectrosc.* 51(11), 1648-1655.
- Ben Sghaier, A. E. O., Chaabouni, Y., Msahli, S., and Sakli, F. (2012). "Morphological and crystalline characterization of NaOH and NaOCl treated *Agave americana* L. fiber," *Industrial Crops and Products* 36(1), 257-266.
- Chu, L.-Q., Masyuko, R., Sweedler, J. V., and Bohn, P. W. (2010). "Base-induced delignification of *Miscanthus x giganteus* studied by three-dimensional confocal raman imaging," *Bioresour. Technol.* 101(13), 4919-4925.
- Ciesielski, P. N., Resch, M. G., Hewetson, B., Killgore, J. P., Curtin, A., Anderson, N., Chiaramonti, A. N., Hurley, D. C., Sanders, A., and Himmel, M. E. (2014). "Engineering plant cell walls: Tuning lignin monomer composition for deconstructable biofuel feedstocks or resilient biomaterials," *Green Chemistry* 16(5), 2627-2635.
- Donaldson, L. A. (2001). "Lignification and lignin topochemistry—An ultrastructural view," *Phytochemistry* 57(6), 859-873.
- Donaldson, L. A., and Knox, J. P. (2012). "Localization of cell wall polysaccharides in normal and compression wood of radiata pine: Relationships with lignification and microfibril orientation," *Plant Physiology* 158(2), 642-653.
- Gierlinger, N., and Schwanninger, M. (2006). "Chemical imaging of poplar wood cell walls by confocal Raman microscopy," *Plant Physiology* 140(4), 1246-1254.
- Grabber, J. H. (2005). "How do lignin composition, structure, and cross-linking affect degradability? A review of cell wall model studies," *Crop Science* 45(3), 820-831.
- Grethlein, H. E. (1985). "The effect of pore size distribution on the rate of enzymatic hydrolysis of cellulosic substrates," *Nat. Biotechnol.* 3(2), 155-160.
- Hänninen, T., Kontturi, E., and Vuorinen, T. (2011). "Distribution of lignin and its coniferyl alcohol and coniferyl aldehyde groups in *Picea abies* and *Pinus sylvestris* as observed by Raman imaging," *Phytochemistry* 72(14), 1889-1895.
- Hoffmann, P., and Parameswaran, N. (1976). "On the ultrastructural localization of hemicelluloses within delignified tracheids of spruce," *Holzforschung* 30(2), 62-70.
- Holopainen-Mantila, U., Marjamaa, K., Merali, Z., Käsper, A., Bot, P. D., Jääskeläinen, A.-S., Waldron, K., Kruus, K., and Tamminen, T. (2013). "Impact of hydrothermal pre-treatment to chemical composition, enzymatic digestibility and spatial distribution of cell wall polymers," *Bioresour. Technol.* 138, 156-162.
- Kumar, R., Mago, G., Balan, V., Wyman, C.E. (2009). "Physical and chemical characterizations of corn stover and poplar solids resulting from leading pretreatment technologies," *Bioresour. Technol.* 100(17), 3948-3962.
- Ma, J., Zhou, X., Zhang, X., and Xu, F. (2013). "Label-free in situ Raman analysis of opposite and tension wood in *Populus nigra*," *BioResources* 8(2), 2222-2233.
- McIntosh, S., and Vancov, T. (2011). "Optimisation of dilute alkaline pretreatment for enzymatic saccharification of wheat straw," *Biomass Bioenergy* 35(7), 3094-3103.
- Mosier, N., Wyman, C., Dale, B., Elander, R., Lee, Y., Holtzapple, M., and Ladisch, M. (2005). "Features of promising technologies for pretreatment of lignocellulosic biomass," *Bioresour. Technol.* 96(6), 673-686.
- Murnen, H. K., Balan, V., Chundawat, S. P., Bals, B., Sousa, L. D. C., and Dale, B. E. (2007). "Optimization of ammonia fiber expansion (AFEX) pretreatment and enzymatic hydrolysis of *Miscanthus x giganteus* to fermentable sugars," *Biotechnol. Progr.* 23(4), 846-850.

- Nlewem, K. C., and Thrash Jr., M. E. (2010). "Comparison of different pretreatment methods based on residual lignin effect on the enzymatic hydrolysis of switchgrass," *Bioresour. Technol.* 101(14), 5426-5430.
- Pauly, M., and Keegstra, K. (2008). "Cell-wall carbohydrates and their modification as a resource for biofuels," *The Plant Journal* 54(4), 559-568.
- Peng, F., and Westermarck, U. (1997). "Distribution of coniferyl alcohol and coniferaldehyde groups in the cell wall of spruce fibres," *Holzforschung* 51(6), 531-536.
- Persson, T., Ren, J. L., Joelsson, E., and Jönsson, A.-S. (2009). "Fractionation of wheat and barley straw to access high-molecular-mass hemicelluloses prior to ethanol production," *Bioresour. Technol.* 100(17), 3906-3913.
- Saha, B. C., and Cotta, M. A. (2006). "Ethanol production from alkaline peroxide pretreated enzymatically saccharified wheat straw," *Biotechnol. Progr.* 22(2), 449-453.
- Sendich, E. N., Laser, M., Kim, S., Alizadeh, H., Laureano-Perez, L., Dale, B., and Lynd, L. (2008). "Recent process improvements for the ammonia fiber expansion (AFEX) process and resulting reductions in minimum ethanol selling price," *Bioresour. Technol.* 99(17), 8429-8435.
- Shomer, I., Frenkel, H., and Polinger, C. (1991). "The existence of a diffuse electric double layer at cellulose fibril surfaces and its role in the swelling mechanism of parenchyma plant cell walls," *Carbohydr. Polym.* 16(2), 199-210.
- Somerville, C., Bauer, S., Brininstool, G., Facette, M., Hamann, T., Milne, J., Osborne, E., Paredes A., Persson, S., and Raab, T. (2004). "Toward a systems approach to understanding plant cell walls," *Science* 306(5705), 2206-2211.
- Ucar, G. (1990). "Pretreatment of poplar by acid and alkali for enzymatic hydrolysis," *Wood Sci. Technol.* 24(2), 171-180.
- Varga, E., Szengyel, Z., and Réczey, K. (2002). "Chemical pretreatments of corn stover for enhancing enzymatic digestibility," *Appl. Biochem. Biotechnol.* 98(1-9), 73-87.
- Vian, B. (1982). "Organized microfibril assembly in higher plant cells," in: *Cellulose and Other Natural Polymer Systems*, R. M. Brown (ed.), Plenum, New York.
- Wang, Z., Li, R., Xu, J., Marita, J. M., Hatfield, R. D., Qu, R., and Cheng, J. J. (2012). "Sodium hydroxide pretreatment of genetically modified switchgrass for improved enzymatic release of sugars," *Bioresour. Technol.* 110(54), 364-370.
- Wiley, J. H., and Atalla, R.H. (1987). "Band assignments in the Raman spectra of celluloses," *Carbohydr. Res.* 160(2), 113-129.
- Yang, B., and Wyman, C. E. (2006). "BSA treatment to enhance enzymatic hydrolysis of cellulose in lignin containing substrates," *Biotechnol. Bioeng.* 94(4), 611-617.
- Zhang, Z., Ma, J., Ji, Z., and Xu, F. (2012). "Comparison of anatomy and composition distribution between normal and compression wood of *Pinus bungeana* Zucc. revealed by microscopic imaging techniques," *Microsc. Microanal.* 18(6), 1459-1468.

Article submitted: January 17, 2014; Peer review completed: March 3, 2014; Revised version received and accepted: May 16, 2014; Published: May 20, 2014.